LANGMUIR Article
Cite This: Langmuir 2018, 34, 10287−10292
pubs.acs.org/Langmuir

Effect of Cell Inner Pressure on Deposition Volume in Microinjection

Xian Wang,[†,‡,#] Qili Zhao,[†,#] Li Wang,[†] Jun Liu,[†] Huayan Pu,[§] Shaorong Xie,[§] Changhai Ru,[∥] and Yu Sun*[,†,‡,⊥]

[†]Department of Mechanical and Industrial Engineering, University of Toronto, Toronto M5S 3G8, Canada
[‡]Institute of Biomaterials and Biomedical Engineering, University of Toronto, Toronto M5S 3G9, Canada
[§]School of Mechatronic Engineering and Automation, Shanghai University, Shanghai 200072, China
[∥]Research Center of Robotics and Micro System & Collaborative Innovation Center of Suzhou Nano Science and Technology, Soochow University, Suzhou, Jiangsu 215021, China
[⊥]Department of Electrical and Computer Engineering, University of Toronto, Toronto M5S 3G4, Canada

Supporting Information

ABSTRACT: Microinjection is a widely used technique for introducing exogenous materials into cells. Many applications of microinjection, such as gene editing and drug testing, rely on the accurate control of the deposition volume. However, the deposition volume in microinjection is presently calibrated in an open medium without considering the cell inner pressure effect, which we experimentally show in this paper that it can induce an error as large as 30% between the actual deposition volume and the set volume. In this work, the relationship between the cell inner pressure and the deposition volume was analytically modeled and experimentally validated. On the basis of the developed model, the cell inner pressure of a given cell type can be well estimated from the injection pressure and the resulting deposition volume. The quantitated cell inner pressure is then used to reduce the error between the set volume and the actual deposition volume. Experiments conducted on human bladder cancer cells (T24 and RT4) showed that T24 cells have a higher inner pressure than RT4 cells (405 ± 45 Pa vs 341 ± 34 Pa), and after compensating for the cell inner pressure, the error between the intended set volume and the actual deposition volume into a cell became less than 3%.

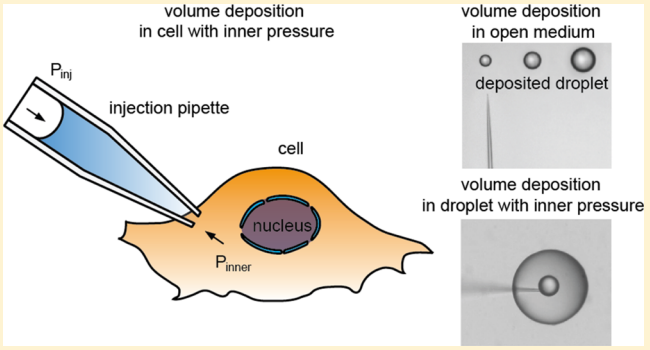

INTRODUCTION

Microinjection is a widely used technique for introducing exogenous materials into cells. It has been used for delivering cDNAs,[1] proteins,[2] peptides,[3] drugs,[4] sperms,[5] and particles[6] into suspended (oocytes[7] and embryos[8,9]) and adherent cells (somatic cells[10] and cultured cells[11]) for gene transfection,[12] for clinical applications (e.g., in vitro fertilization),[13−15] and for studying cell−cell communications[16] and intracellular transport.[17]

The various applications of microinjection rely on the capability of quantitatively controlling the deposition volume.[18] For example, in gene transfection, the amount of introduced genome-editing materials may result in opposite outcomes as upregulation and downregulation of the target gene.[19] In drug screen using microinjection, the dose effect is critical for evaluating the efficacy of a drug.[20] In characterizing cell−cell communications through introducing fluorophores, deposition volume variations can also significantly impact measurement results (Figure 1b).[16,21]

In a microinjection system (Figure 1a), deposition volume control relies on hydraulic or pneumatic pumping. The deposition volume in hydraulic pumping is estimated by measuring the position of the oil−medium interface.[5,22] In comparison, pneumatic microinjection is more commonly used for quantitative deposition volume control because the deposition volume can be conveniently controlled by varying the pneumatic pressure, pulse number, pulse length, and the size of the microinjection opening.[5,18,23] Presently, in the standard practice of pneumatic microinjection, the deposition volume is calibrated by depositing target materials into an open medium [e.g., phosphate-buffered saline (PBS) into mineral oil or vice versa] inside a Petri dish until a measurable volume is reached (Figure 1c), during which values of parameters such as micropipette's tip size, pneumatic pressure, pulse width, and number of pulses are determined. The negligence of the cell inner pressure (osmotic pressure) in the calibration process significantly affects the actual deposition volume inside a cell because material deposition in microinjection is inherently a

Received: June 20, 2018
Revised: August 1, 2018
Published: August 10, 2018

DOI: 10.1021/acs.langmuir.8b02102
Langmuir 2018, 34, 10287−10292

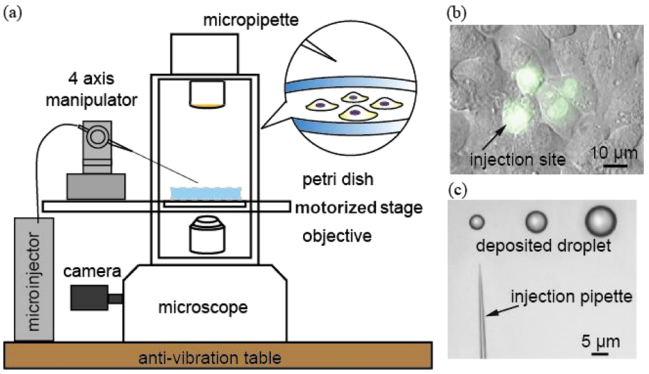

Figure 1. (a) Schematic of a standard microinjection system. (b) Microinjection of fluorescent dyes (exogenous material) into adherent cells for quantifying cell−cell communications. (c) Deposition volume calibration in an open medium in a Petri dish (e.g., PBS is deposited into mineral oil) through applying multiple injection pressure pulses and quantifying the volume of the deposited droplets. The example shown here used an injection micropipette with an inner radius of 150 nm, an injection pressure of 1 kPa, and a pulse duration of 500 ms.

balance between the cell inner pressure and the injection pressure at the tip of the microinjection pipette. For instance, as discussed later in this paper, the actual deposition volume, because of the negligence of the cell inner pressure effect, can be 30% less than the intended set volume using the parameters calibrated in an open medium. This error does not stem from instrument limitations. Commercially available pneumatic microinjection pumps (e.g., Digital Microinjector from Sutter Instrument, PL1-100A from Harvard Apparatus, and PV820 from World Precision Instruments) all have pressure accuracy better than 0.1%. For a typical microinjection pressure of 1 kPa, the error of pressure produced by these pumps is less than 1 Pa, which is negligible compared to typical cell inner pressure values (a few hundreds of pascal).

This work aimed to investigate and compensate for the effect of cell inner pressure on the deposition volume in microinjection. The relationship between the cell inner pressure and the deposition volume was analytically modeled and experimentally validated. For the two types of cells tested in this work, the experimental results show that the human bladder cancer cell T24 (stage III) has a higher inner pressure than the human bladder cancer cell RT4 (stage I), 405 ± 45 Pa versus 341 ± 34 Pa. Experimental results also show that after compensating for the cell inner pressure, the error between the intended set volume and the actual deposition volume into a cell became less than 3%.

EXPERIMENTAL SECTION

Microinjection System and Procedures. The microinjection system used in this work consisted of a standard inverted microscope (Nikon TE2000-S, Nikon Microscopes), a micromanipulator (MX7600, Siskiyou, Inc.), a picoliter pump (Digital Microinjector, Sutter Instrument USA), and a glass micropipette, which was laser-pulled through heating a microfilament to have an outer radius of 250 nm and an inner radius of 150 nm and mounted on the micromanipulator. A camera was connected to the microscope to provide microscopy imaging and visual feedback. A host computer runs our custom-built control software to control all the aforementioned instruments. In experiments, the material to be injected (PBS, mineral oil, dye, etc.) was first back-loaded into the micropipette. The micromanipulator and the $X-Y$ stage were cooperatively controlled for positioning the micropipette along the XYZ axes and positioning cells in the XY plane, respectively. The $X-Y$ stage has a travel range of 75 mm along both axes with a resolution of 0.01 μm and a repeatability of ±1 μm. The micromanipulator has a travel range of 20 mm and a resolution of 0.1 μm along each axis. The micromanipulator was controlled through the custom-built control software to position the micropipette to penetrate the cell membrane, and the pump was controlled to deposit the material loaded in the micropipette into the cell using preset parameters (injection pressure, pulse duration, and pulse number).

Image Processing and Deposition Volume Calculation. The microinjection experiments were conducted, while images/videos were recorded through a Nikon TE2000-S microscope under bright field, using an objective lens of 20× magnification. Because the droplets deposited into cells were largely spherical in shape, the deposition volume was calculated based on the measured diameter of the deposited droplet from the images using edge detection and Hough transform with a subpixel quantification resolution of approximately 0.1 μm. The limitation in imaging resolution for quantifying the deposition volume was further discussed in the Results and Discussions section. Image processing and volume calculation were conducted in MATLAB. The code is available at https://github.com/XianShawn/microinjection.

Cell Lines. Human bladder cancer cells, T24 and RT4, were obtained from the America Type Culture Collection (ATCC, Manassas, VA). Cells were cultured in ATCC-formulated McCoy's 5A modified medium with 10% fetal bovine serum and 1% penicillin−streptomycin at 37 °C and 5% CO_2. Subculture was conducted before the cells reached confluency. Before experiments, T24 and RT4 cells were passaged and seeded at 2500 cells/cm^2 in glass bottom Petri dishes (P35G-1.5-14-C, MatTek Corporation, USA) for 12 h.

Fluorescent Dye. In dye injection experiments for validating membrane sealing immediately after microinjection, the membrane-impermeable 8-hydroxypyrene-1,3,6-trisulfonic acid (HPTS) dye with a concentration of 2 mM (Life Technologies, Burlington, CA) was injected into single cells by using the microinjection system. HPTS was chosen for validating membrane sealing because of its small molecular size (molecular mass: 524.37 Da) and the membrane-impermeable property. HPTS is highly water-soluble; therefore, it does not cause micropipette clogging.

RESULTS AND DISCUSSION

In microinjection processes, the material deposition process relies on the disturbance of force/pressure balancing at the tip of the microinjection pipette. When a pneumatic pressure is applied to push aqueous solution from the micropipette into a cell, the injection force (F_{inj}) is balanced by three forces, including the capillary force (F_c), which arises from intermolecular interactions between the liquid and the surrounding solid surface of the micropipette, the wall-induced force (F_w) due to the radium decrease near the tip of the microinjection pipette, and the force resulting from the cell inner pressure (F_{inner}), as illustrated in Figure 2a. The flow inside the microinjection pipette is assumed to be laminar (see the Supporting Information), and the cell inner pressure is considered to be constant during the microinjection process because the deformable cell membrane with folded structures helps maintain the cell inner pressure when the deposition volume is small[24,25] (<10% of the cell volume[26]).

The force balancing equation for the material inside the injection pipette is

$$F_{inj} = F_c + F_w + F_{inner} \quad (1)$$

where the injection force $F_{inj} = P_{inj}\pi R^2$ with R denoting the inner radius of the micropipette and P_{inj} denoting the microinjection pressure; capillary force $F_c = T2\pi R \cos \alpha$ with T denoting the surface tension between air and water (T = 72.86 mN/m at 20 °C[27]) and α denoting the contact angle at

DOI: 10.1021/acs.langmuir.8b02102
Langmuir 2018, 34, 10287−10292

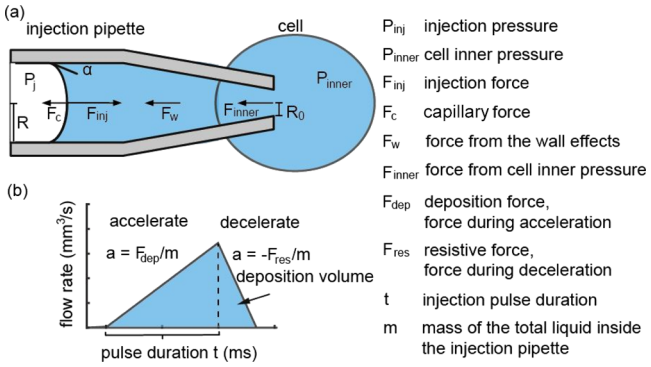

Figure 2. (a) Pressure and force analysis of volume deposition in microinjection. (b) During material deposition, the flow rate of the liquid inside micropipette first increases until the end of the pressure pulse and then decreases until zero.

the air−liquid interface (Figure 2a); $F_w = \pi(R^2 - R_0^2)P_i$ with R_0 denoting the inner radius of the micropipette tip; and the force arising from the cell inner pressure $F_{inner} = P_{inner}\pi R_0^2$.

Substituting the expression of F_{inj}, F_c, F_w, and F_{inner} into the force balancing equation eq 1, the injection pressure in the balanced state is

$$P_{inj} = P_{inner} + \frac{2T\cos\alpha}{R}$$

2

For depositing materials into a cell, the injection force F_{inj} (or injection pressure P_{inj}) must be increased to disrupt force/pressure balancing, namely,

$$F_{inj} > F_c + F_w + F_{inner} \tag{3}$$

$$P_{inj} > P_{inner} + \frac{2T\cos\alpha}{R} \tag{4}$$

When the above conditions are met, the aqueous solution within the micropipette is deposited into the cell that has an inner pressure of P_{inner}.

During the material deposition process, because the injection pressure and the cell inner pressure are constant, the flow rate of the liquid inside the micropipette accelerates and then decelerates linearly until the flow rate decreases to zero (Figure 2b). The deposition volume can be calculated as the integral of the flow rate over time, namely,

$$V = \int Q\,dt = \int v{\cdot}A\,dt \tag{5}$$

where Q is the flow rate, A is the cross-sectional area at the micropipette tip, and v is the flow velocity. As shown in Figure 2b, the area of the blue triangle represents the deposition volume, the maximal flow velocity is $A{\cdot}t\left(\frac{F_{dep}}{m}\right)$, and the total time duration is $\left(2 + \frac{F_{dep}}{F_{res}}\right)$. Thus, the deposition volume is

$$V = \frac{1}{2}{\cdot}tA\left(\frac{F_{dep}}{m}\right){\cdot}t\left(2 + \frac{F_{dep}}{F_{res}}\right) = \frac{\pi R_0^2 t^2}{2\rho V_0}\left(2 + \frac{F_{dep}}{F_{res}}\right)F_{dep} \tag{6}$$

where t is the duration of the injection pressure (i.e., the width of the injection pulse), deposition force $F_{dep} = F_{inj} - (F_c + F_w + F_{inner})$ is the force during the acceleration process, resistive force $F_{res} = F_c + F_w + F_{inner}$ is the force during the deceleration process, and $m = \rho V_0$ is the total mass of the liquid inside the micropipette with ρ denoting the density of the liquid and V_0 representing the total volume of the liquid inside the micropipette.

The ensuing analysis indicates that even the largest F_{dep} is still significantly lower than the smallest F_{res} (i.e., $F_{dep} \ll F_{res}$). With R = 0.1 mm, the inner radius of 100 nm at the micropipette tip (R_0 = 100 nm, extreme case in the range of 100−1000 nm, leading to the smallest F_{res}), injection pressure of 1 kPa (P_j = 1 kPa, extreme case in the range of 1−10 kPa, leading to the smallest F_{res}), injection pulse of 10 ms (t = 10 ms, extreme case in the range of 10−500 ms, leading to the largest F_{dep}), 1 μL water loaded into the micropipette (V_0 = 1 μL and ρ = 1 g/cm^3), the injection force F_{inj} is 3×10^{-3} N, and the resistive force $F_{res} = F_c + F_w + F_{inner}$ is also 3×10^{-3} N, based on force balancing in eq 1. According to eq 6, for the deposition volume in the scale of 0.1 pL (10^{-16} m^3) from each injection pulse, only a small disturbance of the force balancing is required, namely, F_{dep} is very small and equals 3.3×10^{-5} N. Even with extreme values, F_{dep} is only about 1.1% of F_{res} (namely, $F_{dep} \ll F_{res}$). Then, the deposition volume is

$$V = \frac{\pi R_0^2 t^2}{\rho V_0}F_{dep} = \frac{\pi R_0^2 t^2}{\rho V_0}[F_{inj} - (F_c + F_w + F_{inner})]V$$
$$= \frac{\pi^2 R_0^2 R^2 t^2}{\rho V_0}\left(P_{inj} - P_{inner} - \frac{2T\cos\alpha}{R}\right) \tag{7}$$

Thus, the deposition volume linearly depends on the injection pressure and the cell inner pressure.

To experimentally validate the relationship between the inner pressure and the deposition volume shown in eq 7, we microinjected mineral oil (M8410, Sigma-Aldrich, USA) into hemispherical water droplets that were of different sizes and have different inner pressures. The hemispherical water hemispherical droplets were formed through depositing water into a Petri dish full of oil. The larger density of water than oil and the hydrophobic interface between oil and water result in hemispherical water droplets of different sizes (10 pL, 50 pL, 100 pL, 500 pL, 1 nL, and 10 nL) immersed in oil. On the basis of the Young−Laplace equation, the inner pressure (P_{inner}) of the hemispherical water droplet is

$$P_{inner} = \frac{2T}{R_{droplet}} \tag{8}$$

where T is the surface tension between mineral oil and water (50 mN/m at 20 °C) and $R_{droplet}$ is the radius of the hemispherical water droplet. With a set volume of 0.5 pL, oil was then microinjected into the hemispherical water droplets that were of different sizes, and the actual deposition volume of oil was measured. The error bars in Figure 3b represent standard deviation of five repeated measurements in independent experiments. The measurement uncertainty of the hemispherical water droplets' radius was ~0.2 μm because of the resolution limitation of the imaging setup. The experimentally measured results (Figure 3b) revealed a strong correlation (correlation coefficient R > 0.95) with the model-calculated values using eq 7. It can be seen that when the inner pressure was zero (red arrow in Figure 3b), the set volume was well deposited. However, as the inner pressure became higher, the actually deposited volume further deviated from the set volume, proving the importance of taking the inner pressure

DOI: 10.1021/acs.langmuir.8b02102
Langmuir 2018, 34, 10287−10292

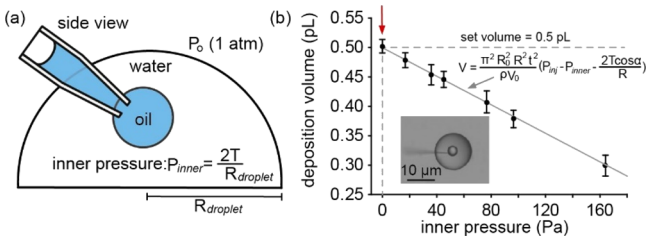

Figure 3. (a) Experimentally created water hemispherical droplets that have different sizes, hence different inner pressures. The water hemispherical droplets were formed inside a Petri dish full of oil. The inner pressure P_{inner} within a water hemispherical droplet is the pressure difference across the water−oil interface caused by surface tension. P_o is the pressure from the medium (i.e., surrounding oil), which is the standard atmospheric pressure. The microinjection-deposited oil droplet is significantly smaller than the hemispherical water droplet (<5% in volume), although the schematic exaggerates the size of the oil droplet for clarity. (b) Experimental results. In all experiments, the set volume was the same (0.5 pL), the injection pressure: 1 kPa, and the inner radius of the micropipette: 150 nm. The red arrow points to the scenario when oil was microinjected into a dish of water, mimicking the situation of zero inner pressure. In all other cases, oil was microinjected into hemispherical water droplets of varying sizes. For each size of a hemispherical water droplet (i.e., for each inner pressure), five individual oil droplets were formed via microinjection and measured. Error bar: standard deviations.

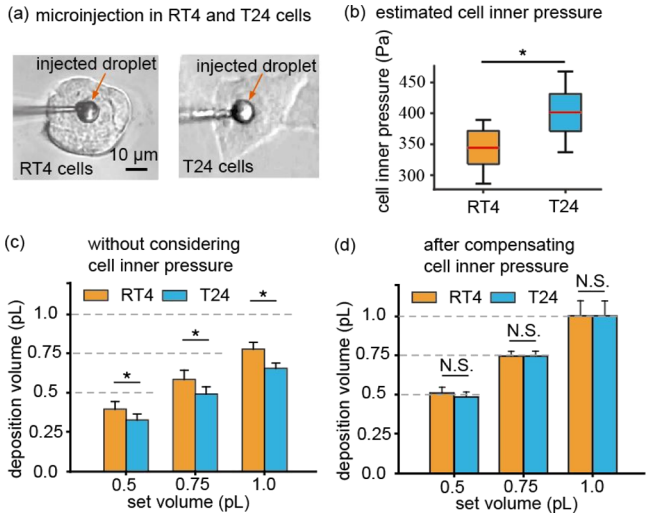

Figure 4. (a) Injection of mineral oil into RT4 and T24 cells. The deposition volume was quantified by measuring the size of the deposited mineral droplet inside the cell. (b) Experimentally quantified inner pressure of RT4 and T24 cells, error bar: standard deviation, n = 20, P < 0.05. (c) Deposition volume vs set volume, without compensating for the cell inner pressure, mean ± standard deviation, n = 15 cells for each set volume, P < 0.05. (d) Deposition volume vs set volume, with the compensation of the cell inner pressure, mean ± standard deviation, n = 15 cells for each set volume, P > 0.05.

into account in order to achieve accurate deposition volumes in microinjection.

Different types of cells possess different inner pressures. When a cell transports materials (e.g., water and ions) from its extracellular environment through the cell membrane into the cell, an osmotic pressure is created. In this work, we tested two human bladder cancer cell lines (stage I: RT4 cells and stage III: T24 cells). According to eq 7, the cell inner pressure P_{inner} can be quantified through measuring the deposited volume V with known injection pressure P_{inj}, pulse duration t, and injection pipette geometries R and R_o. Figure 4a shows the microinjection of mineral oil into individual cells. The volume of the deposited mineral oil droplet was unambiguously measured. Thus, the inner pressures of RT4 cells and T24 cells were experimentally determined to be 341 ± 34 and 405 ± 45 Pa, respectively (n = 20 cells for each cell type) (Figure 4b). Although variances of the cell inner pressure across cells within each cell type exist, they are not significant compared to the difference between the two cell types (P < 0.05). For both cell types, the standard deviation is ~10% of the average cell inner pressure, indicating that the variance may cause ~10% difference in the deposition volume across the cells in the same type of cell, according to the linear relationship between the deposition volume and the cell inner pressure in eq 7. The deposition volume error caused by the inner pressure variance within the same cell type is discussed later in the paper.

In addition, we tested whether microinjection disrupts the cell inner pressure. The membrane-impermeable fluorescent dye (HPTS, ThermoFisher) was injected into both RT4 and T24 cells (n = 20 cells for each cell type). After the micropipette was retracted out of the cell, fluorescence imaging was performed for 10 min, throughout which the deposited dye was contained completely within the cell, and no dye/signal was found outside the cell near the micropipette penetration site (Figure S1). We also immersed RT4 and T24 cells in the membrane impermeable dye (trypan blue solution 0.4%, ThermoFisher), and no dye was observed within the cells after microinjection. These results imply that microinjection with a sharp micropipette (outer radius of 250 nm) does not disrupt the inner pressure because of the cell membrane's strong capability for rapid sealing.[28]

A set volume of 0.5, 0.75, and 1 pL mineral oil was targeted for deposition into RT4 and T24 cells, without considering the cell inner pressure. In experiments, all parameters including P_{inj}, t, V_0, R_0, and R were precalibrated in an open medium without considering the cell inner pressure, according to the presently used standard microinjection volume calibration procedures. P_{inj} = 1 kPa, V_0 = 1 μL, R_0 = 150 nm, and R = 250 nm were kept the same for all experiments. The pulse duration t was set, according to the results of calibration in an open medium, as 10.3 ms for 0.5 pL, 12.6 ms for 0.75 pL, and 14.5 ms for 1 pL. On the basis of eq 7, the deposition volume linearly depends on the term $P_{inj} - P_{inner}$. When a higher injection pressure P_{inj} is used, the effect from the cell inner pressure P_{inner} on the deposition volume becomes smaller. However, a higher injection pressure causes higher shear inside the cell during material deposition, resulting in lower cell viability after microinjection. Therefore, increasing P_{inj} should not be set too high in practice, and an injection pressure in the scale of 1 kPa is commonly used. The experimental results are summarized in Figure 4c. Significant errors between the deposition volume and the set volume were observed as 20.1%, 21.8%, and 22.0% for the set volume of 0.5, 0.75, and 1 pL, respectively, for RT4 cells and 34.2%, 34.0%, and 34.8% for the set volume of 0.5, 0.75, and 1 pL, respectively, for T24 cells. The resulting deposition volume also showed significant differences between the two types of cells (RT4 vs T24: 0.40 ± 0.04 pL vs 0.32 ± 0.04 pL, 0.59 ± 0.06 pL vs 0.49 ± 0.04 pL, 0.78 ± 0.04 pL vs 0.66 ± 0.04 pL, P < 0.05, n = 12 cells for each cell type and for each set volume).

DOI: 10.1021/acs.langmuir.8b02102
Langmuir 2018, 34, 10287−10292

Table 1. Differences between the Actual Deposition Volume and the Set Volume

	set volume (pL)					
	without considering the cell inner pressure			after the cell inner pressure compensation		
cell type	0.5	0.75	1.0	0.5	0.75	1.0
RT4	0.10 ± 0.04	0.16 ± 0.06	0.22 ± 0.04	0.00 ± 0.04	0.00 ± 0.05	0.03 ± 0.08
T24	0.18 ± 0.04	0.26 ± 0.04	0.34 ± 0.04	0.01 ± 0.05	0.10 ± 0.05	0.02 ± 0.09

Next, according to the linear relationship between the deposition volume and the cell inner pressure in eq 7, we compensated for the cell inner pressure for deposition volume control via adding the estimated cell inner pressure as an offset to the injection pressure P_{inj}. The compensated injection pressure, P_{inj} + 341 Pa, was applied to the microinjection of RT4 cells, and P_{inj} + 405 was applied to the microinjection of T24 cells (P_{inj}= 1 kPa). After this pressure compensation (V_0, R_0, and R values were unchanged, t was still set as 10.3 ms for 0.5 pL, 12.6 ms for 0.75 pL, and 14.5 ms for 1 pL), as summarized in Figure 4d, the error between the mean deposition volume and the set volume for all the three set volumes (0.5, 0.75, and 1 pL) became less than 3% for RT4 cells and less than 2% for T24 cells. The resulting deposition volume showed no significant difference between the two types of cells (RT4 vs T24: 0.50 ± 0.04 pL vs 0.51 ± 0.05 pL, 0.75 ± 0.05 pL vs 0.75 ± 0.05 pL, 1.03 ± 0.08 pL vs 1.02 ± 0.09 pL, P > 0.05, n = 15 cells for each cell type and for each set volume). The remaining 3 and 2% errors between the mean deposition volume and the set volume can be attributed to the error in the quantitation of the deposition volume for the inner pressure measurement, limited by the imaging resolution (0.2 μm). The difference of deposition volume between RT4 and T24 cells was no longer significant after compensating for the inner pressure difference between two cell types using the mean value (Table 1). The resulting deposition volume had an approximately 10% variance, which can be attributed to the 10% variance in the cell inner pressure across the cells within the same cell type. Despite the variance of the inner pressure across the cells within the same cell type, using the mean inner pressure of the cell type for compensating for the injection pressure is an effective approach for reducing the error between the set volume and the deposition volume for individual cells.

CONCLUSIONS

In summary, many biology experiments based on microinjection rely on accurate deposition volume control in order to quantify the dose effect. Our work, for the first time, proved that the present standard microinjection volume calibration approach can cause the actual deposition volume in a cell to be 30% less than the intended set volume using microinjection parameters calibrated in an open medium without considering the cell inner pressure. The guideline for significantly reducing this error is, after determining the values of microinjection parameters in an open medium, to add the cell inner pressure to the calibrated injection pressure. Instead of trial and error for tuning the deposition volume, applying the developed model provides a quantitative value for compensating for the deposition volume error. In addition, for different experimental conditions (cell type, inner diameter of injection pipette, set volume, etc.), a quantitative pressure offset value can be readily set with the developed model after the cell inner pressure is determined. The experimental results of this work revealed that the use of the compensated injection pressure can effectively reduce the 30% volume error to less than 3%. Equation 7 provides a practical and convenient approach for quantitatively determining the inner pressure of a cell.

ASSOCIATED CONTENT

Supporting Information

The Supporting Information is available free of charge on the ACS Publications website at DOI: 10.1021/acs.langmuir.8b02102.

Dye deposition in RT4 and T24 cells (PDF)

AUTHOR INFORMATION

Corresponding Author

*E-mail: sun@mie.utoronto.ca.

ORCID

Xian Wang: 0000-0002-1501-2544

Li Wang: 0000-0002-5166-0397

Author Contributions

#X.W. and Q.Z. contributed equally to this work. X.W., Q.Z., and Y.S. designed the project. X.W., Q.Z., and L.W. conducted the experiments and processed the data. Y.S., H.P., S.X., and C.R. planned and supervised the work. X.W., Q.Z., and J.L. developed the theoretical model. H.P., S.X., and C.R. verified the model. X.W. and Y.S. drafted the manuscript. All authors discussed the results and contributed to the construction of the manuscript.

Notes

The authors declare no competing financial interest.

ACKNOWLEDGMENTS

The authors thank the financial support from the Canadian Institutes of Health Research (CIHR) and the Natural Sciences and Engineering Research Council of Canada (NSERC) through a CHRP grant, the Ontario Centres of Excellence through an OJIRDP grant, and the Canada Research Chairs Program. The authors also thank the financial support from the National Natural Science Foundation of China (Grant No. 61774107).

REFERENCES

(1) Zhang, Y.; Yu, L.-C. Single-cell microinjection technology in cell biology. *BioEssays* **2008**, *30*, 606−610.

(2) Zhang, Y.; McLaughlin, R.; Goodyer, C.; LeBlanc, A. Selective cytotoxicity of intracellular amyloid β peptide1−42 through p53 and Bax in cultured primary human neurons. *J. Cell Biol.* **2002**, *156*, 519−529.

(3) Pitchiaya, S.; Heinicke, L. A.; Park, J. I.; Cameron, E. L.; Walter, N. G. Resolving subcellular miRNA trafficking and turnover at single-molecule resolution. *Cell Rep.* **2017**, *19*, 630−642.

(4) Brennan, L. D.; Roland, T.; Morton, D. G.; Fellman, S. M.; Chung, S. Y.; Soltani, M.; Kevek, J. W.; McEuen, P. M.; Kemphues, K. J.; Wang, M. D. Small molecule injection into single-cell C. elegans

DOI: 10.1021/acs.langmuir.8b02102
Langmuir 2018, 34, 10287−10292

embryos via carbon-reinforced nanopipettes. *PLoS One* **2013**, *8*, No. e75712.
(5) Permana, S.; Grant, E.; Walker, G. M.; Yoder, J. A. A review of automated microinjection systems for single cells in the embryogenesis stage. *IEEE ASME Trans. Mechatron.* **2016**, *21*, 2391−2404.
(6) Wang, X.; Luo, M.; Wu, H.; Zhang, Z.; Liu, J.; Xu, Z.; Johnson, W.; Sun, Y. A three-dimensional magnetic tweezer system for intraembryonic navigation and measurement. *IEEE Trans. Robot.* **2018**, *34*, 240−247.
(7) Liu, X.; Sun, Y. Microfabricated glass devices for rapid single cell immobilization in mouse zygote microinjection. *Biomed. Microdevices* **2009**, *11*, 1169−1174.
(8) Huang, H. B.; Sun, D.; Mills, J. K.; Cheng, S. H. Robotic cell injection system with position and force control: Toward automatic batch biomanipulation. *IEEE Trans. Robot.* **2009**, *25*, 727−737.
(9) Wang, G.; Xu, Q. Design and development of a piezo-driven microinjection system with force feedback. *Adv. Robot.* **2017**, *31*, 1349.
(10) Yang, C.; Xie, Y.; Liu, S.; Sun, D. Force Modeling, Identification, and Feedback Control of Robot-Assisted Needle Insertion: A Survey of the Literature. *Sensors* **2018**, *18*, 561.
(11) Wang, W.; Sun, Y.; Zhang, M.; Anderson, R.; Langille, L.; Chan, W. A system for high-speed microinjection of adherent cells. *Rev. Sci. Instrum.* **2008**, *79*, 104302.
(12) Gopalakrishnan, B.; Wolff, J. siRNA and DNA transfer to cultured cells. *Methods in Molecular Biology*; Humana Press, 2009; pp. 31-52.
(13) Liu, J.; Shi, C.; Wen, J.; Pyne, D.; Liu, H.; Ru, C.; Luo, J.; Xie, S.; Sun, Y. Automated vitrification of embryos: A robotics approach. *IEEE Robot. Autom. Mag.* **2015**, *22*, 33−40.
(14) Zhang, Z.; Liu, J.; Wang, X.; Zhao, Q.; Zhou, C.; Tan, M.; Pu, H.; Xie, S.; Sun, Y. Robotic Pick-and-Place of Multiple Embryos for Vitrification. *IEEE J. Robot. Autom. Lett.* **2017**, *2*, 570−576.
(15) Lu, Z.; Zhang, X.; Leung, C.; Esfandiari, N.; Casper, R. F.; Sun, Y. Robotic ICSI (intracytoplasmic sperm injection). *IEEE Trans. Biomed. Eng.* **2011**, *58*, 2102−2108.
(16) Liu, J.; Siragam, V.; Gong, Z.; Chen, J.; Fridman, M. D.; Leung, C.; Lu, Z.; Ru, C.; Xie, S.; Luo, J.; Hamilton, R. M.; Sun, Y. Robotic Adherent Cell Injection for Characterizing Cell-Cell Communication. *IEEE Trans. Biomed. Eng.* **2015**, *62*, 119−125.
(17) Koike, S.; Jahn, R. Probing and manipulating intracellular membrane traffic by microinjection of artificial vesicles. *Proc. Natl. Acad. Sci. U.S.A.* **2017**, *114*, No. E9883.
(18) Chow, Y. T.; Chen, S.; Wang, R.; Liu, C.; Kong, C.-W.; Li, R. A.; Cheng, S. H.; Sun, D. Single cell transfection through precise microinjection with quantitatively controlled injection volumes. *Sci. Rep.* **2016**, *6*, 24127.
(19) Khan, A. A.; Betel, D.; Miller, M. L.; Sander, C.; Leslie, C. S.; Marks, D. S. Transfection of small RNAs globally perturbs gene regulation by endogenous microRNAs. *Nat. Biotechnol.* **2009**, *27*, 549−555.
(20) Klinghoffer, R. A.; Bahrami, S. B.; Hatton, B. A.; Frazier, J. P.; Moreno-Gonzalez, A.; Strand, A. D.; Kerwin, W. S.; Casalini, J. R.; Thirstrup, D. J.; You, S.; Morris, S. M.; Watts, K. L.; Grenley, M. O.; Tretyak, I.; Dey, J.; Carleton, M.; Beirne, E.; Pedro, K. D.; Ditzler, S. H.; Girard, E. J.; Deckwerth, T. L.; Bertout, J. A.; Meleo, K. A.; Filvaroff, E. H.; Chopra, R.; Press, O. W.; Olson, J. M. A technology platform to assess multiple cancer agents simultaneously within a patient's tumor. *Sci. Transl. Med.* **2015**, *7*, 284ra58.
(21) Krutovskikh, V. A.; Piccoli, C.; Yamasaki, H. Gap junction intercellular communication propagates cell death in cancerous cells. *Oncogene* **2002**, *21*, 1989−1999.
(22) Reyes, D. R.; Iossifidis, D.; Auroux, P.-A.; Manz, A. Micro total analysis systems. 1. Introduction, theory, and technology. *Anal. Chem.* **2002**, *74*, 2623−2636.
(23) Sive, H. L.; Grainger, R. M.; Harland, R. M. Defolliculation of Xenopus Oocytes. *Cold Spring Harb. Protoc.* **2010**, *2010*, prot5535.
(24) Diz-Muñoz, A.; Fletcher, D. A.; Weiner, O. D. Use the force: membrane tension as an organizer of cell shape and motility. *Trends Cell Biol.* **2013**, *23*, 47−53.
(25) Jiang, H.; Sun, S. X. Cellular pressure and volume regulation and implications for cell mechanics. *Biophys. J.* **2013**, *105*, 609−619.
(26) Guillaume-Gentil, O.; Potthoff, E.; Ossola, D.; Dörig, P.; Zambelli, T.; Vorholt, J. A. Force-controlled fluidic injection into single cell nuclei. *Small* **2013**, *9*, 1904−1907.
(27) Pallas, N. R.; Harrison, Y. An automated drop shape apparatus and the surface tension of pure water. *Colloids Surf.* **1990**, *43*, 169−194.
(28) Steinhardt, R. A.; Bi, G.; Alderton, J. M. Cell membrane resealing by a vesicular mechanism similar to neurotransmitter release. *Science* **1994**, *263*, 390.

DOI: 10.1021/acs.langmuir.8b02102
Langmuir 2018, 34, 10287−10292